The Richer Representation the Better Registration

Mohammad Rouhani, Angel Domingo Sappa

The Richer Representation the Better Registration

Mohammad Rouhani, *Student Member, IEEE*, and Angel Domingo Sappa, *Senior Member, IEEE*

***Abstract*— In this paper, the registration problem is formulated as a point to model distance minimization. Unlike most of the existing works, which are based on minimizing a point-wise correspondence term, this formulation avoids the correspondence search that is time-consuming. In the first stage, the target set is described through an implicit function by employing a linear least squares fitting. This function can be either an implicit polynomial or an implicit B-spline from a coarse to fine representation. In the second stage, we show how the obtained implicit representation is used as an interface to convert point-to-point registration into point-to-implicit problem. Furthermore, we show that this registration distance is smooth and can be minimized through the Levengberg–Marquardt algorithm. All the formulations presented for both stages are compact and easy to implement. In addition, we show that our registration method can be handled using any implicit representation though some are coarse and others provide finer representations; hence, a tradeoff between speed and accuracy can be set by employing the right implicit function. Experimental results and comparisons in 2D and 3D show the robustness and the speed of convergence of the proposed approach.**

***Index Terms*— Rigid registration, surface fitting, implicit polynomials, implicit B-splines, registration error estimation, residual error minimization, Levenberg-Marquadt algorithm.**

I. Introduction

OBJECT representation and point set registration both are common problems in computer vision. In general, they are tackled as standalone problems and studied separately. The current work places a bridge that connects both problems looking for an efficient solution. Being inspired by the Computer Graphics (CG) and Computer Aided Design (CAD) communities a compact object representation is adopted to reformulate the registration problem in a unified *representation-registration* framework.

The object representation field focuses on developing compact models that allow to deal with large amount of data. Nowadays, due to the improvement in 3D scanners, we are surrounded by a high amount of raw data as 2D or 3D cloud of points, and having a smooth and compact representation is one of the important objectives that benefit computer vision applications. In the current work we exploit implicit representations, including Implicit Polynomial (IP) and Implicit B-Spline (IBS), to tackle the registration of two clouds of points.

The registration problem, on the other hand, aims at finding the best transformation that places both the given source set and its corresponding target set into the same reference system in order to minimize their distance. This transformation, depending on the application, could be either rigid or non-rigid. The rigid transformation only considers rotation and translation parameters to move the source set [1]. The non-rigid transformation, on the contrary, allows more degrees of freedom for deforming the source set in order to minimize the distance between the two sets [2], [3]. The current work presents a novel rigid registration distance approximation that can benefit both rigid and non-rigid registration. It is an extension of a preliminary version [4] where only IPs are used to describe the target set. In this work we show that the proposed point to model distance minimization can be also used with a more flexible implicit representation, Implicit B-Spline (IBS) [5]. This flexible representation (IBS) can be used to induce a fast and robust registration error.

The best rotation and translation could be roughly approximated by the Principle Component Analysis (PCA). Indeed, PCA just finds the major axes of each cloud of points and then aligns these axes by translating the origin followed by a rotation; hence, it just provides a coarse registration. The registration methods, in general, can be divided into two main categories, namely *coarse* and *fine* registration, where the latter provides a more precise alignment. The coarse registration is not very precise but it can be used as initialization for a fine registration method. Gelfand et. al. in [6], for instance, present a coarse registration using a branch-and-bound algorithm to initialize a fine registration algorithm.

In general, fine registration approaches find the best rigid transformation by iterating two steps. In the first step the correspondences between the given source points and the target points are sought in order to compute the registration residual error. Then, in the second step, the best set of parameters are found by minimizing this residual error. These two steps are repeated until some convergence criteria is reached. The Iterative Closest Point (ICP) algorithm is one of the classical registration approaches following this two-step scheme. It has been originally presented in [7] and [11] and several improvements have been proposed in the literature looking for more efficient and robust solutions (e.g., [8]–[10]). Note that in most of these approaches the correspondence search is performed at the point level and it makes the whole process computationally expensive.

Some effort to link the registration with the representation problem has been made by using high level representations in order to avoid the correspondence search. Implicit polynomials have been exploited in [11] to represent both the source set and

Manuscript received January 2, 2013; revised June 3, 2013 and July 31, 2013; accepted August 24, 2013. Date of publication September 11, 2013; date of current version October 2, 2013. This work was supported by the Government of Spain under Projects TIN2011-25606 and TIN2011-29494-C03-02. The associate editor coordinating the review of this manuscript and approving it for publication was Prof. Gang Hua.

M. Rouhani is with Morpheo, INRIA Rhône-Alpes, Grenoble 38000, France (e-mail: mohammad.rouhani@inria.fr).

A. D. Sappa is with the Computer Vision Center, Bellaterra 08193, Spain (e-mail: angel.sappa@cvc.uab.es).

Color versions of one or more of the figures in this paper are available online at http://ieeexplore.ieee.org.

Digital Object Identifier 10.1109/TIP.2013.2281427

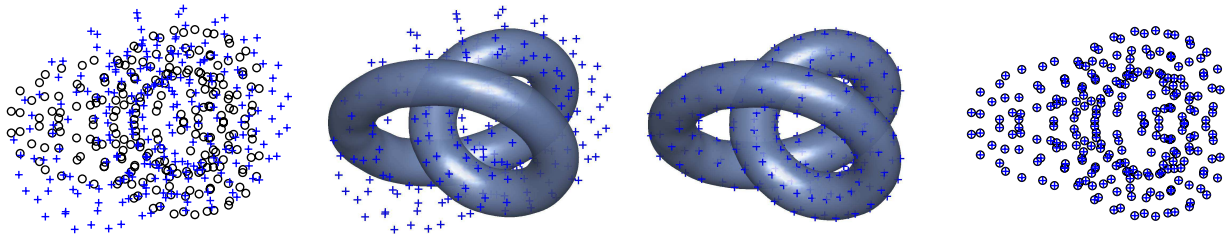

Fig. 1. Using an interface for point sets registration: (*a*) Initial position of source (+) and target (o) sets; (*b*) Source set (+) and target set represented by an IBS; (*c*) Registration result of source set (+) and the IBS; (*d*) The same result but represented by using the target set (o) and transformed source set (+).

target set. Probabilistic representations, like GMM, have been used to describe both source set and target set (e.g. [12]–[14]). In [15]–[17] the point-wise problem is avoided by using either the distance field of the target set or the distance fields of both target and source sets. More details about all these approaches are given in the next section.

The current work proposes a novel and fast registration approach that exploits a compact and smooth representation as an interface to avoid the point-to-point correspondence search. It consists of two main stages: in the first stage, an implicit representation is provided to describe the target set. An optimal implicit function is fitted using the least squares form, hence it is quite fast. Although any implicit function can be used in the current work we just show the usage of implicit polynomials and implicit B-splines, which can be indistinctly adopted in the proposed registration framework. In the second stage, we use a fast distance estimation to define the residual errors. This distance is induced by the fitted implicit function from the first stage. The final registration distance is differentiable with respect to the registration parameters and allows solving the problem through a gradient based optimization algorithm. Due to the compactness of the implicit representation the whole scheme can be used in a coarse-to-fine framework. The rest of this paper is organized as follows: Section II details related work. Section III presents both the proposed representation and registration approaches. Experimental results and comparisons with state of the art are presented in Section IV. Finally, conclusions are given in Section V.

II. Motivation and Related Work

Let us consider two sets of points, referred to as source set (*data*) $\mathcal{S} = \{s_i\}_1^{N_s}$, and target set (*model*) $\mathcal{T} = \{t_i\}_1^{N_t}$ (see Fig. 1(*a*)). In the rigid case, the registration problem aims at finding the best rotation and translation in order to take the source set as *close* as possible to the target set. For this purpose many point-to-point comparisons must be executed in order to measure the closeness. For the non-structured case it will take $O(N_s N_t)$ just for obtaining the distance measurement. Although more elaborated solutions using data structure have been introduced, our proposal is to replace the target set with a proper *interface* that accelerates the distance measurement (Fig. 1). Then the optimal configuration can be found through measuring the point distances from this interface.

In order to work with an interface, instead of a point cloud, a proper geometric model should be used. Triangle meshes and parametric NURBS are among the common tools in these domains, but they suffer from either the geometry limitation or the parametrization problem. Implicit functions, on the contrary, provide a flexible representation without requiring any parametrization over the point cloud. They describe objects in 2D/3D through the level set where the function reaches zero. Implicit Polynomial (IP) [18] is one of the simplest choices for the function space $\mathcal{F}$, since it is made out of simple monomials. IPs can easily describe a given object through a set of coefficients, but they are not flexible enough. In other words, IPs suffer from the outliers created around the point set, which are due to their non-compact supports. Radial Basis Functions (RBFs) [19] provide another solution space for implicit representations. They are smooth and flexible, but small changes in the coefficient vector can lead to a global change in the whole object.

In this work Implicit B-Splines (IBSs) beside implicit polynomials are employed to represent the target set. IBS proposes a smooth and flexible representation without any need of parametrization [20]. Moreover, it is constructed out of B-spline basis functions, which have compact supports. Hence they have local control (i.e, changes in one coefficient changes the local behavior of the object). Fig. 1(*b*) illustrates the flexibility of IBSs to describe a complex 3D shape. In the current work the optimal IBS/IP is easily obtained by means of an extension of the 3L algorithm [18], which is a fast algebraic fitting method formulated as linear least squares.

IP and IBS both provide an overall representation for the target points. Since both are in a linear implicit form, they can be easily computed. IP provides a fast and simple representation while IBS results in a more accurate description. Once the target set has been described by a proper implicit function the registration problem can be tackled in a point-to-model scheme, which leads to a correspondence free registration method. Moreover, a tradeoff between the speed and accuracy can be met by employing a coarse or fine implicit representation. Point-to-model schemes have been already studied in the literature by considering different representations for target and source sets. These methods can be broadly classified as probabilistic-based and distance-field-based approaches.

Probabilistic approaches represent each given set by a probabilistic model like multivariate t-distributions [12] or Gaussian Mixture Model (GMM) [13], [21]; hence, the

registration problem becomes a problem of aligning two mixtures, which can be solved in the quasi-Newton optimization framework. These approaches are highly dependent on the number of mixtures used for modeling the point sets. Hence, a user defined number of mixtures, or as many as the number of points, is required. Moreover, although these methods do not require any correspondence search, all points in the model are implicitly considered as a potential correspondence (almost all the points contribute to the GMM construction).

On the contrary to the previous approaches, distance field has been used as an implicit representation, which provides information over the whole domain. The method presented in [15] overcomes the non-differentiable nature of ICP by using a differentiable distance transform—Chamfer distance. The error function derived from that distance field is a smooth function, and its derivatives can be analytically computed; hence it can be minimized through the Levenberg-Marquardt algorithm (LMA) to find the optimal registration parameters. The distance field used in [15] is a discrete field and its derivatives used in LMA are not precise enough. In [16] a local quadratic approximation of the distance function, based on the curvature information, is presented. Unfortunately, computing the principal curvatures over the point cloud is computationally expensive and sensitive to noise. Finally, [17] proposes a distance field approximation by using an implicit polynomial [22]. This IP is considered to define a gradient flow that drives the source towards the target without using point-wise correspondences. Although fast, the proposed gradient flow is not precise, especially close to the boundaries.

In the current work a novel approach is presented to reformulate the point-to-point registration as a *point-to-model* problem. In the first stage, an implicit function is constructed to represent the target points. This representation is either an implicit polynomial or implicit B-spline that can be rapidly constructed. As a contribution a linear least squares fitting algorithm is adopted to find the optimal IBS that describes the target set more accurate than IP. Fig. 1(a) illustrates the initial position of the source and target sets. The IBS zero set representing the given target set is depicted in Fig. 1(b). In the second stage this implicit function (either IP or IBS) is used as an interface during the registration process. Fig. 1(c) presents the registration results from the source set and the IBS. Note that the optimal registration result is obtained as shown in Fig. 1(d). In this figure source set and target set are depicted again as point clouds.

III. Proposed Method

This section presents the main contributions of the current work. First, the target set is described through an implicit function like implicit polynomial (IP) or implicit B-spline (IBS). We employ the 3L algorithm to find the optimal IP and adapt it to find the optimal IBS. IP and IBS are both in implicit forms so the target points are not required to be parametrized. Moreover, both classes are linear with respect to their coefficient vectors; so, we employ the same technique to find an optimal IP or IBS. In the second part, the obtained implicit representation is used for aligning two sets of points. The distance used to measure the alignment error is a fast distance estimation induced by the fitted implicit function. The accumulated error is in the non-linear least squares form, and hence can be optimized by the Levenberg-Marquadt Algorithm. This minimization stage is iterated until convergence is reached. It should be highlighted that the formulations presented in the second stage are completely independent of the choice for the representation in the first stage. So, it is up to the user to chose either a simple and fast representation like IP or a more flexible and precise one like IBS.

A. Object Representation

An object in 2D/3D can be easily described by a cloud of points sampled from the object surface. This point cloud can be enriched by knowing the point connections, for instance through the corresponding triangle mesh. Unfortunately, this representation has a geometry limitation and requires lots of memory to deliver a fine enough representation. Moreover, point level representation induces expensive point-wise computations for our registration problem. In order to cope with these limitations, the target point cloud is described through an implicit function. An implicit function f describes the object of interest implicitly through its *zero set* including those points where f obtains zero; i.e., $Z_f = \{\mathbf{x} \in \mathbb{R}^k : f(\mathbf{x}) = 0\}$. Given the target points $\mathcal{T} = \{t_i\}_1^{N_t}$ an optimal implicit function can be sought by minimizing the distance between the target points and the zero set of this function. This implicit function f can be easily chosen as an implicit polynomial defined as:

$$f(\mathbf{x}) = f(x, y) = \sum_{\substack{(i+j)\leqq d \\ \{i,j\}\geqq 0}} c_{i,j} x^i y^j = 0, \tag{1}$$

where d is the polynomial degree. An IP is a simple description of the point set through a set of monomials and coefficients. The higher the IP degree is the more degree of freedom are captured by the IP; but then, the outliers created by the IP zero set cannot be easily avoided. In our experiments we use an IP up to 7th degree that can roughly describe the point cloud. In order to have a finer and precise representation, an implicit B-Spline can be alternatively used, which is defined as a combination of the tensor products of 1D basis functions:

$$f(\mathbf{x}) = f(x, y) = \sum_{i=1}^{M} \sum_{j=1}^{N} c_{i,j} B_i(x) B_j(y), \tag{2}$$

where $B_i(x)$ $B_j(y)$ are the spline basis functions, and the matrix $[c_{i,j}]_{M\times N}$ is the control lattice (coefficients) controlling the shape of the IBS [5]. For the sake of simplicity we consider $M = N$, then the basis functions $B_i(x)$ and $B_j(y)$ have the same behavior, though defined in different domains. Similarly, the basis functions in 3D are tensor products of three 1D basis functions. In general, IBSs provide smooth and flexible representations in an implicit form. Constructed through a set of basis functions with compact supports, IBS can be locally controlled in contrast to implicit polynomials and radial basis functions.

We exploit the simplicities and flexibilities of IPs and IBSs to reformulate the registration problem. In the first stage of our

registration method the target set is replaced by an IP or IBS by employing the same fitting algorithm. It should be noticed that IP and IBS, despite their different formulations, have a similar form and both of them can be linearly described based on the their coefficients:

$$f(\mathbf{x}) = \mathbf{c}^T \mathbf{m}(\mathbf{x}) = \mathbf{m}(\mathbf{x})^T \mathbf{c}, \tag{3}$$

where $\mathbf{c}$ is the coefficient vector containing the IP or IBS coefficients and $\mathbf{m}(\mathbf{x})$ is the basis vector containing the IP or IBS basis functions. The basis vector for IP comprises the monomials in the form of $x^i y^j$:

$$\mathbf{m}(\mathbf{x}) = [1, x, y, x^2, xy, y^2, x^3, x^2y, ..., y^d]^T. \tag{4}$$

For the case of implicit B-Spline the basis vector contains the basis functions in the term of tensor products $B_i(x)B_j(y)$:

$$\mathbf{m}(\mathbf{x}) = [B_1(x)B_1(y), ..., B_1(x)B_N(y), ..., B_N(x)B_N(y)]^T. \tag{5}$$

Note that the coefficient vector must respect the same order as the basis vector. Then, the inner product of the coefficient vector and the basis vector (either IP or IBS) defines the implicit function (IP/IBS) as already defined in (1) and (2).

Surface reconstruction techniques concern finding the optimal coefficient vectors to describe the given point cloud. In the current work, we employ the 3L algorithm [18] to find the optimal coefficients in order to describe the target point cloud $\mathcal{T} = \{t_i\}_1^{N_t}$. Moreover, we adapt the original algorithm to find the optimal IBS coefficients still in a linear least squares framework. The decision whether to use IP or IBS to represent the given target set depends on its geometrical complexity. In other words, the user should select which one is the best option for the given target set: if a simple overall description is enough, then IP can be used; otherwise, IBS is preferred in order to capture more details of target point cloud. In this section we show that a common fitting framework and formulation can be used to find the optimal IP or IBS description and this is why we present both formulations at the same time. Later in section III-B we show that our proposed formulation for point to model registration is independent of the implicit representation of the target points, so both IP and IBS can be used. Of course employing a low resolution IP during the registration leads us to a coarse solution, while a high resolution IBS (afterwards) can deliver a better estimation of the registration parameters.

The 3L algorithm considers the given target points $\mathcal{T}_0 = \mathcal{T}$ as well as its inner and outer offsets $\{\mathcal{T}_{+\delta}, \mathcal{T}_{-\delta}\}$. The optimal function f (either IP or IBS) is found such that it obtains zero in the original set as well as $\pm\epsilon$ in the additional offsets. Then, the objective function $F(\mathbf{c}) = \|\mathbf{M}_{3L}\mathbf{c} - \mathbf{b}\|^2$ is considered to be minimized, where:

$$\mathbf{M}_{3L} = \begin{bmatrix} \mathbf{M}_{\mathcal{T}_{-\delta}} \\ \mathbf{M}_{\mathcal{T}_0} \\ \mathbf{M}_{\mathcal{T}_{+\delta}} \end{bmatrix}, \quad \mathbf{b} = \begin{bmatrix} -\epsilon \\ \mathbf{0} \\ +\epsilon \end{bmatrix}. \tag{6}$$

The monomial matrices $\mathbf{M}_{\mathcal{T}_0}$ and $\mathbf{M}_{\mathcal{T}_{\pm\delta}}$ are constructed from the basis vectors computed in the original set $\mathcal{T}_0$ and its offsets $\mathcal{T}_{\pm\delta}$ respectively. In fact each row in these matrices is made out of the basis functions presented in (4) or (5) depending on whether IP or IBS is selected for the description.

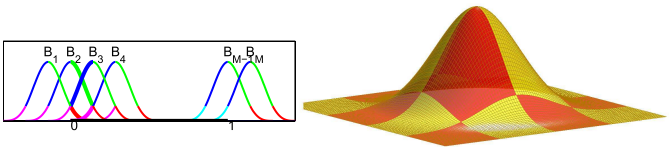

Fig. 2. Cubic B-Spline basis functions: ($left$) 2D basis functions made out of blending functions; ($right$) a tensor product 3D basis functions defined on the unit square.

The 3L algorithm is originally proposed for Implicit Polynomials [18]. In order to adapt the 3L formulation for IBS solution space, the monomial matrix $\mathbf{M}_{3L}$ must be constructed for the IBS case. Referring to (6), this matrix contains the basis vectors computed in the original source set, the inner and outer offsets. The basis vector at a given point constructing a row of $\mathbf{M}_{3L}$ is computed through the definition in (5). The way in which the value of basis functions is computed is based on the blending functions that are defined on [0, 1]. Without loss of generality, through this paper a cubic B-Spline formulation is used, which is made out of the following patches:

$$\begin{aligned} b_0(u) &= (1-u)^3/6, \quad b_1(u) = (3u^3 - 6u^2 + 4)/6, \\ b_2(u) &= (-3u^3 + 3u^2 + 3u + 1)/6, \quad b_3(u) = u^3/6. \end{aligned} \tag{7}$$

These cubic patches blend together leading to C^2 continuous basis functions. Fig. 2 shows how a B-Spline is defined out of these *blending functions*. In order to have N basis functions in the interval [0, 1] the step of the *knot*[1] sequence is uniformly chosen with the step of $\Delta = 1/(N-3)$ (see Fig. 2($left$)). This sequence is chosen in order to cover the whole unit interval, then the tensor product in 2D (3D) covers the whole unit square (cube). It should be emphasized that the implicit B-spline, unlike the parametric B-splines or NURBS, does not impose any parametrization over the given point set. So the knot sequence in this context is not related to any parametrization over the point set. It is simply related to the space where the given points are coming from. In our implementation we normalize all the data to put them in a unit square (cube).

Considering the cubic B-spline with a uniform knot sequence the definition in (2) can be directly reformulated based on the blending functions:

$$f(\mathbf{x}) = f(x, y) = \sum_{r=0}^{3}\sum_{s=0}^{3} c_{i+r,j+s} b_r(u).b_s(v) \tag{8}$$

where the indices start from:

$$i = \lfloor x/\Delta \rfloor + 1, \quad j = \lfloor y/\Delta \rfloor + 1 \tag{9}$$

and the given coordinates in XY will be mapped in UV as:

$$\begin{aligned} u &= x/\Delta - \lfloor x/\Delta \rfloor, \\ v &= y/\Delta - \lfloor y/\Delta \rfloor. \end{aligned} \tag{10}$$

This definition provides us with the computational efficiency useful for calculating the monomial matrix and the regularization term that is presented later in this section. The basis vector for a given point in M_{3L} should be computed through the

[1]knot: position where two blending functions join.

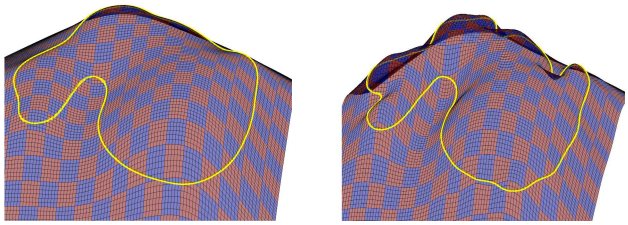

Fig. 3. Illustrations of the fitted IBS with different regularization (μ in (13)); resulting zero sets are highlighting.

definition in (8). Note that the value $b_r(u)b_s(v)$ corresponds to the term $B_{i+r}(x)B_{j+s}(y)$ in the basis vector $\mathbf{m}(\mathbf{x})$ and it will be used to fill in the proper entry according to (5). Once the M_{3L} is constructed (either for IP or IBS), the optimal implicit coefficients can be directly computed as the least squares solution:

$$\mathbf{c} = \mathbf{M}_{3L}^{\dagger}\mathbf{b} = (\mathbf{M}_{3L}^{T}\mathbf{M}_{3L})^{-1}\mathbf{M}_{3L}^{T}\mathbf{b}. \tag{11}$$

The matrix $\mathbf{M}_{3L}^{T}\mathbf{M}_{3L}$ in (11) is very close to be singular and especially for the case that IBS is a highly sparse matrix. This problem can be addressed by some regularization techniques like Ridge Regression (RR). In the current work a geometric meaningful tension term is considered instead to regularize the control parameters [20]. This term is computed by measuring the curvature of the hyper-surface f over the whole domain:

$$T(\mathbf{c}) = \iint_{XY} f_{xx}^2 + 2f_{xy}^2 + f_{yy}^2 dxdy. \tag{12}$$

Considering the vector form of IBS in (3) this tension term can be written as $\mathbf{c}^T\mathbf{H}\mathbf{c}$, which is a quadratic function of the control value. Thus the minimization problem is updated as:

$$F(\mathbf{c}) = \|\mathbf{M}_{3L}\mathbf{c} - \mathbf{b}\|^2 + \mu\mathbf{c}^T\mathbf{H}\mathbf{c}, \tag{13}$$

where μ controls the regularization smoothness. Fig. 3, for instance, shows how the regularization value controls the smoothness of the shape. The optimal solution of (13) can be obtained by solving a linear system of equations [20]:

$$\mathbf{c} = (\mathbf{M}_{3L}^{T}\mathbf{M}_{3L} + \mu\mathbf{H})^{-1}\mathbf{M}_{3L}^{T}\mathbf{b}, \tag{14}$$

It should be noticed that the matrix $\mathbf{H}$ can be directly constructed based on the blending functions defining the spline basis functions.

The formulation presented in (14) is common for both IP and IBS; the only difference is the way the monomial matrix $\mathbf{M}_{3L}$ is constructed. For the case of IP it is simply filled in with rows of monomials while in the case of IBS it is made out of the right product of b-spline patches. Moreover, typical IP fitting methods use a simple regularization matrix like the identity matrix $\mathbf{H} = \mathbf{I}$ (ridge regression) that has no geometric interpretation, while in our case we use a tension term that controls the rigidity of the implicit function. Finally, we should highlight that no parametrization is imposed on the target points and the order of points injected in the monomial matrix does not affect the optimal value for the coefficient vector.

B. Objects Alignment

The implicit representation computed in (14) provides a smooth description of the target points through its zero set. As mentioned in the previous section it can be either an IP or an IBS with different degrees or different regularization effects. A low degree IP, for instance, delivers an overall description for the target points while a higher degree IP captures more details in the target; however, the degree can be automatically set [22]. Once the target point set is replaced with a proper implicit function, the point-to-point registration is converted into a point-to-model registration, which can be considered in different resolutions. Moreover, the implicit representation provides information over the whole space that can be useful. In fact, the values of implicit function around the object boundary provide good approximations of the distance function. In this subsection we describe how the implicit representation is exploited to measure and minimize the registration error.

1) Distance Formulation: in the rigid case, the registration approaches search for the optimal set of parameter Θ, which contains rotation angles and translation. In 2D case the rigid transformation contains three parameters $\Theta = [\theta, \mathbf{t_x}, \mathbf{t_y}]^{\mathrm{T}}$ and in 3D case it contains six parameters $\Theta = [\theta, \phi, \psi, \mathbf{t_x}, \mathbf{t_y}, \mathbf{t_z}]^{\mathrm{T}}$; the first three for rotation and the last three for translation. The optimal parameter vector $\hat{\Theta}$ moves the source points $\mathcal{S} = \{s_i\}_1^{N_s}$ as close as possible to the interface $f_{\mathbf{c}}(\mathbf{x})$ that describes the target points $\mathcal{T}$:

$$\hat{\Theta} = argmin_{\Theta}\left(\sum_{i=1}^{N_d} Dist^2(\mathbf{R}s_i + \mathbf{t}, f_{\mathbf{c}})\right), \tag{15}$$

where $Dist$ is a function that measures the distance between the source points and the implicit function. In this distance estimation all the source points are considered. In order to lessen the effect of outliers we should discard some of the source points [23]. For instance, it can be 10% of the points with the largest distances. In a more elaborated fashion, we can simply reach the set of inlier indices $\mathcal{I}$ by discarding those source points with a distance beyond $2\sigma_d$, i.e., $\mathcal{I} := \{i | Dist(\mathbf{R}s_i + \mathbf{t}, f_{\mathbf{c}}) < 2\sigma_d\}$, where σ_d is the standard deviation of the distances [24].

In the current work this distance is approximated using the estimation proposed in [25] that is an estimation of the orthogonal distance based on the first order Taylor expansion of the distance function; hence, it can be easily computed by normalizing the algebraic distance by the gradient norm:

$$Dist(s, f_{\mathbf{c}}) \approx \frac{|f_{\mathbf{c}}(s)|}{||\nabla f_{\mathbf{c}}(s)||}. \tag{16}$$

This estimation is interesting since it is: i) independent of the zero set representation; and ii) invariant to rigid body transformation. Using this approximation in (15), the registration parameters can be found by minimizing the following function:

$$\begin{aligned} Dist_{\Theta} &= \sum_{i\in\mathcal{I}}\left(\frac{f_{\mathbf{c}}(\mathbf{R}s_i + \mathbf{t})}{\| \nabla f_{\mathbf{c}}(\mathbf{R}s_i + \mathbf{t}) \|}\right)^2 \\ &= \sum_{i\in\mathcal{I}}(w_i f_{\mathbf{c}}(\mathbf{R}s_i + \mathbf{t}))^2 = \sum_{i\in\mathcal{I}} d_i^2, \end{aligned} \tag{17}$$

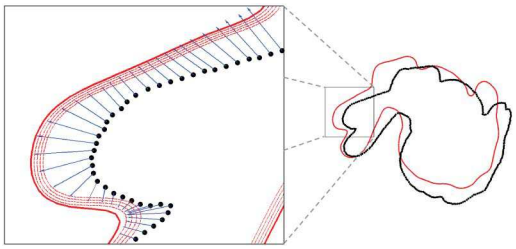

Fig. 4. The level curves of the IBS is used to approximate the distance. In addition, the distance sensitivity with respect to small changes in rotation and translation can be approximated as well.

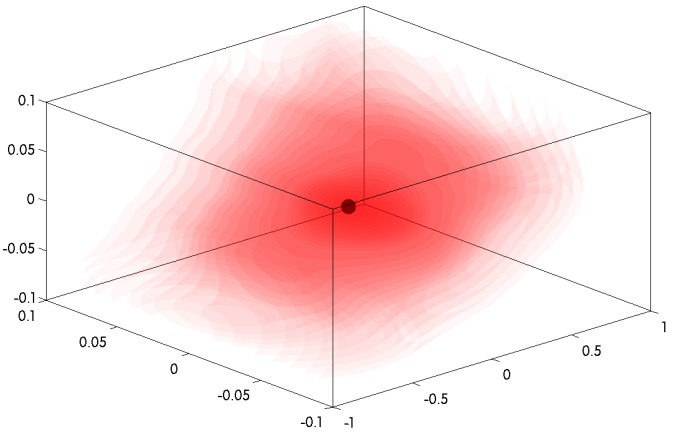

Fig. 5. Convergence region of the proposed approach with respect to $[\theta, \mathbf{t_x}, \mathbf{t_y}]$ for the 2D object and IBS in Fig. 11(*top*).

where:

$$d_i = w_i f_{\mathbf{c}}(\mathbf{R}s_i + \mathbf{t}), \qquad (18)$$
$$w_i = 1/\| \nabla f_{\mathbf{c}}(\mathbf{R}s_i + \mathbf{t}) \|,$$

represent the distance of transformed source point and the proper weight to approximate it. Thus, the point-to-point registration is tackled in a higher level using a curve or surface as an interface. This interface provides a rich structure for the registration process, together with advantages like robustness to noise and missing data. Fig. 4 illustrates how this interface facilitates the registration error estimation without any need to correspondence search.

2) Distance Optimization: the proposed registration distance is smooth and differentiable with respect to the registration parameters (see Fig. 5). Moreover, the gradient information of this distance can be analytically calculated. Hence it can be used in any gradient based optimization algorithm like gradient descent and Levenberg−Marquardt algorithm (LMA). Intuitively, the gradient information of this distance function shows its sensitivity with respect to rigid parameters.

In this work we use LMA for the optimization part [26], which is particularly proposed for non-linear least squares forms as the case in (17). This method proposes a tradeoff between the gradient descent and the Gauss−Newton algorithm. In order to handle LMA, the value of each residual in (17) and its partial derivatives, which are expressed in a *Jacobian* matrix J, must be provided. Since LMA uses the gradient information and the first order distance approximation in (17) captures this information, higher degree approximations would not benefit the result of LMA. It should be mentioned that the derivatives of summands in (17) must be calculated with respect to the parameters in Θ. Hence, the Jacobian matrix consisting of three columns in 2D case and six columns in 3D case can be easily computed. Since the implicit function $f_{\mathbf{c}}$ is a smooth function, w_i could be considered as a constant weight, hence its derivative vanishes. As a general formula each entry of the Jacobian matrix can be computed as an inner product:

$$\mathbf{J}(i, j) = w_i \left(\frac{\partial}{\partial \Theta_j} (\mathbf{R}s_i + \mathbf{t}) \right) . \nabla f(\mathbf{R}s_i + \mathbf{t}), \qquad (19)$$

where Θ_j is the jth parameter of Θ. This matrix contains 3 or 6 columns for the case of 2D or 3D respectively. Those rows of $\mathbf{J}$ corresponding to outliers ($i \notin \mathcal{I}$) should be removed. The derivatives of the transformed source points in (19) can be analytically computed. For instance for 2D case we have:

$$\frac{\partial}{\partial \Theta_1} (\mathbf{R}s_i + \mathbf{t}) = \begin{pmatrix} -\sin(\theta) & -\cos(\theta) \\ \cos(\theta) & -\sin(\theta) \end{pmatrix} s_i \qquad (20)$$

$$\frac{\partial}{\partial \Theta_2} (\mathbf{R}s_i + \mathbf{t}) = \mathbf{e_1} \quad \frac{\partial}{\partial \Theta_3} (\mathbf{R}s_i + \mathbf{t}) = \mathbf{e_2} \qquad (21)$$

where $\mathbf{e_1}$ and $\mathbf{e_2}$ are the unit basis vectors.

Having estimated the proposed distance (17) and its Jacobian matrix through (19) it is easy to perform LMA in order to refine the rigid parameter vector Θ:

$$\Theta^{k+1} = \Theta^k + \beta \triangle \Theta,$$
$$(\mathbf{J}^{\mathrm{T}}\mathbf{J} + \lambda diag(\mathbf{J}^{\mathrm{T}}\mathbf{J})) \triangle \Theta = \mathbf{J}^{\mathrm{T}}\mathbf{D}, \qquad (22)$$

where β is the refinement step; $diag(\mathbf{J}^{\mathrm{T}}\mathbf{J})$ is the diagonal matrix containing the diagonal entries of $(\mathbf{J}^{\mathrm{T}}\mathbf{J})$; $\triangle\Theta$ represents the refinement vector for the rigid parameters; λ is the damping parameter in LMA; and the vector $\mathbf{D}$ is a column vector containing the values $Dist(\mathbf{R}s_i + \mathbf{t}, f_{\mathbf{c}})$ in the current rotation $\mathbf{R}$ and translation $\mathbf{t}$. In our implementation they are initialized as $\theta = 0$, $\mathbf{t_x} = 0$ and $\mathbf{t_y} = 0$; more evolved initializations, such as PCA alignment, could be alternatively used. Parameter refinement (22) in LMA must be repeated till convergence is reached.

Fig. 5 shows an illustration of the convergence region of the proposed registration framework. This region corresponds to the 2D bunny shape case study and its fitting IBS shown in Fig. 11(*top*). The axes on this plot correspond to $[\theta, \mathbf{t_x}, \mathbf{t_y}]$ parameters. This figure depicts that the proposed registration method converges to the optimal parameter (the point shown in the center) independently of the initialization in the region (relative position of source and target sets). Different layers in this 3D plot correspond to level surfaces with similar distance values. Our experimental results show that the regularization parameter used during fitting has impact on the convergence region. Indeed a larger regularization parameter leads to a coarser and smoother implicit representation, and a wider convergence region as a consequence.

IV. Experimental Results and Comparisons

The experimental results are presented for the proposed registration scheme using different implicit representations. In the first section, simple IPs are considered to represent the target sets. Despite the simplicity of the representation the obtained registration results are quite promising. In the following section this representation is promoted to IBSs that provide more flexible representations to tackle the registration of objects with intricate and challenging geometries like the ones presented in Fig. 1 and Fig. 12. Note that a single IP, independently of its degree, cannot properly capture the geometry of a complex object, such as the one presented in Fig. 1, which as a consequence will affect the registration result.

The proposed approach has been evaluated using different 2D and 3D source sets and target sets from public repositories [27] and [28]. In all the examples, just to visually appreciate the result, the same set of points is used as source and target sets. Notice that the proposed approach does not consider the points in the target set during the registration, despite that after the registration the source points appear on the target points.

In addition to the qualitative evaluation presented with 2D contours 3D real objects have been registered with the proposed approach and compared with four techniques (i.e., [13], [15]–[17]) from the state of the art, together with the classical ICP [7]. Each technique iterates until one of these stopping criteria is reaches: if the number of iterations exceeds a maximum bound (#Iter $= 40$) or the relative registration error is smaller than the given threshold ($\epsilon < 0.005$); relative registration error is defined as: $\epsilon = |E_t - E_{t-1}|/E_t$, where E_t refers to the registration error between the target and source set at iteration t.

On the contrary to the relative registration error, which is an internal measure, an *Accumulated Residual Error* (ARE) is used during the comparisons. It is computed by measuring the accumulated error, in a point-wise manner, from the transformed source set to a *reference set*. This reference set corresponds to a highly detailed description of the target set. It contains the target set and on average is defined by a set of points ten times larger than the target set. Each residual error is computed by finding the nearest point in between the registered source set and the reference set.

A. Registration Using IPs

In this section, point-to-point registration problem is converted to point-to-IP registration that can be solved faster; ideally, it is intended for 2D contours or 3D objects with simple geometries. Fig. 6 shows initial configurations for four different source and target sets. The first row corresponds to closed contours with a full overlap. Source sets have been obtained by rotating and translating the corresponding target set, and by adding Gaussian noise to study the robustness of all the techniques. Accuracy and number of iterations are provided in Table I and Table II respectively. It should be highlighted that the proposed approach converges in all the cases and most of the time with the smallest error and lowest

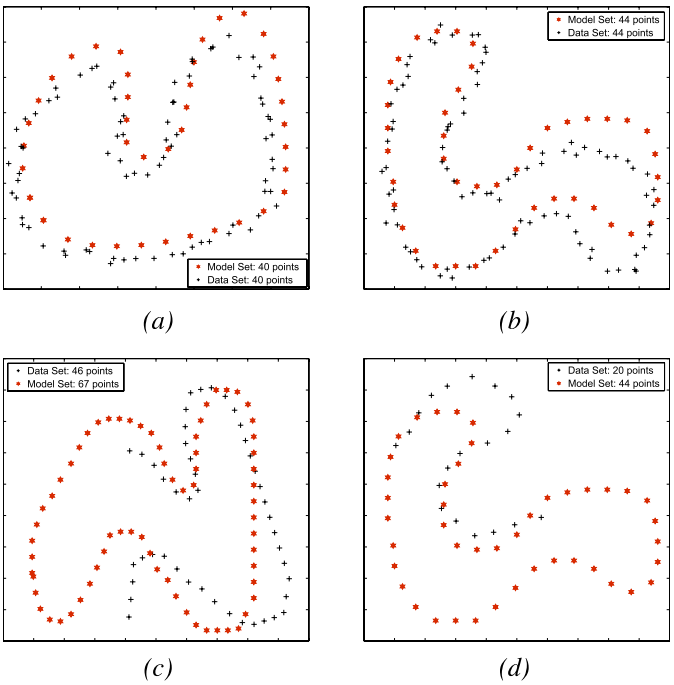

Fig. 6. Initial positions of data sets and target sets for noisy ((*a*) and (*b*)) and partial overlap ((*c*) and (*d*)) examples registered with the different approaches.

number of iterations, in spite of the noise in the source set. In these examples IPs of degree six have been used for fitting the target sets. The IP degree could be automatically determined through the algorithm in [22], which is based on the QR decomposition of the monomial matrix. Fig. 6 (*bottom*) presents two examples where the source set partially overlaps the corresponding target set; source and target sets correspond to uniform sampling of different boundaries. Target points have been fitted by sixth degree IPs in both cases. Both of them have been registered using the proposed technique and the five aforementioned ones; the obtained registration accuracy is given in the third and fourth rows of Table I, as well as the number of iterations when one of the stopping criteria is reached.

Fig. 7 presents challenging situations where target sets and source sets contain different densities of points. Fig. 7(*left*) shows the initial configurations while Fig. 7(*right*) depicts the results obtained by using the proposed approach. Quantitative results from these two examples are presented in Table I and Table II. The challenge in these examples lie on the non-existence of any point to point correspondence, although both clouds of points correspond to the same contor. The proposed approach, since the target set is represented by a unified IP, is robust in this kind of situations.

In addition to 2D cases presented above, 3D real objects from public data sets [27] and [28] have been registered with the proposed approach and compared with state of the art techniques. The first column in Fig. 8 shows initial position of source and target sets both represented by means of triangular meshes to highlight the details. The second column depicts IPs describing the target points together with the points of their corresponding source sets and the third one is the final regis-

TABLE I

COMPARISONS OF REGISTRATION ERROR (ARE) RESULTS FOR 2D CASES (ICP: ITERATIVE CLOSEST POINT [7]; GMM: GAUSSIAN MIXTURE MODELS [13]; DT: DISTANCE TRANSFORM [15]; GF: GRADIENT FLOW [17]; DA: DISTANCE APPROXIMATION [16]; PA: PROPOSED APPROACH)

	ICP	GMM	DT	GF	DA	PA
Fig. 6(a)	1.62	2.32	1.65	1.64	1.65	**1.59**
Fig. 6(b)	1.41	1.34	1.42	1.42	1.40	**1.32**
Fig. 6(c)	0.91	5.11	4.00	0.98	0.92	**0.53**
Fig. 6(d)	0.52	1.75	0.20	0.29	0.35	**0.18**
Fig. 7(a)	0.26	0.89	0.39	0.48	0.42	**0.19**
Fig. 7(c)	1.54	2.48	0.57	1.92	1.22	**0.34**

TABLE II

NUMBER OF ITERATIONS OF DIFFERENT REGISTRATION METHODS FOR 2D CASES

	ICP	GMM	DT	GF	DA	PA
Fig. 6(a)	*13*	*13*	*25*	*27*	*11*	***4***
Fig. 6(b)	*10*	*7*	*28*	*15*	*9*	***6***
Fig. 6(c)	*7*	*10*	*30*	*16*	*10*	***9***
Fig. 6(d)	***13***	*18*	*27*	*20*	*17*	*15*
Fig. 7(a)	*14*	*10*	*29*	*12*	*13*	***11***
Fig. 7(c)	*16*	*13*	*30*	*28*	***12***	*13*

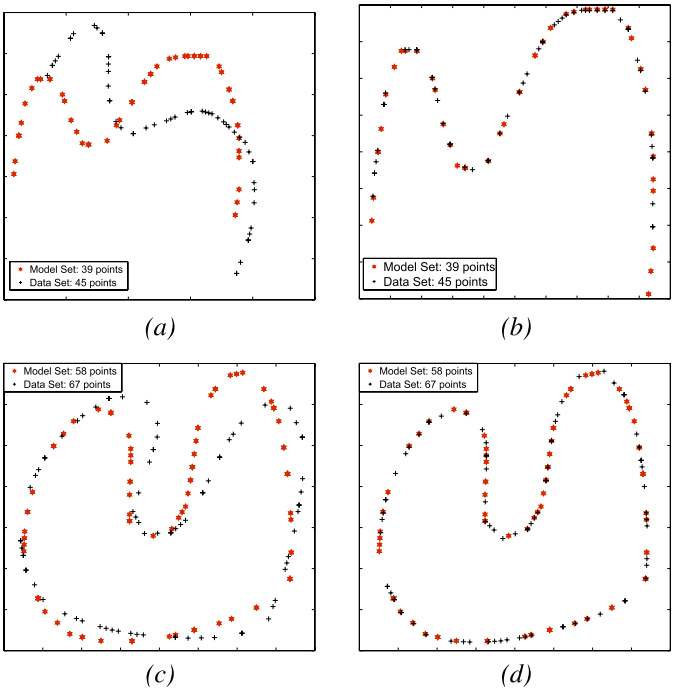

Fig. 7. Source and target sets containing different density of points. ((*a*) and (*b*)) Initial configurations. ((*c*) and (*d*)) Final results from the proposed approach.

Fig. 8. Public data sets (from [27] and [28]) registered with the proposed approach and state of the art techniques. (*a*) Initial set up of the given source and target sets represented by means of triangular meshes to highlight details. (*b*) IPs representing target sets and source points. (*c*) Results of the proposed registration approach represented through triangular meshes to make visual evaluation easier.

tration result. The illustration presented in Fig. 8(a)($1^{st}row$) corresponds to a source set defined by 811 points. The target contains 926 points and is represented by means of a seventh degree IP. The result obtained with the proposed approach is shown in Fig. 8(c)($1^{st}row$). Quantitative information about the data sets, as well as comparisons with other approaches are provided in Table III; the stopping criteria considered in Table I are also used here. A seventh degree IP is used in the second row to represent the 745 points of the target set, while the source set contains 609 points. Note that after describing the target set with its fitting IP the target points are no longer considered. A fifth degree and a sixth degree IPs are used in the third and fourth rows, respectively. Fig. 8(c) presents the registration obtained with the proposed approach. Statistics about their registration process and comparisons with state of the art techniques are presented in Table III and Table IV.

Finally, two cases where the source and target are partially overlapped are presented in Fig. 9. The (top) row shows a simple example where the source and target sets are picked from the same ellipsoid, which is described by a second degree IP in the presented approach. These two sets are partially overlapped (about 40%) as shown in the last column. Despite the simplicity of the problem, none of the techniques presented

TABLE III

COMPARISONS OF REGISTRATION ERROR (ARE) RESULTS FOR 3D CASES (ICP: ITERATIVE CLOSEST POINT [7]; GMM: GAUSSIAN MIXTURE MODELS [13]; DT: DISTANCE TRANSFORM [15]; GF: GRADIENT FLOW [17]; DA: DISTANCE APPROXIMATION [16]; PA: PROPOSED APPROACH)

	(N_s,N_t)	ICP	GMM	DT	GF	DA	PA
Fig. 8($1^{st}row$)	(811,926)	3.45	6.30	3.80	**3.37**	3.45	3.38
Fig. 8($2^{nd}row$)	(609,745)	2.84	5.02	2.84	2.75	2.86	**2.74**
Fig. 8($3^{rd}row$)	(625,639)	2.38	4.83	2.35	**1.89**	2.40	1.90
Fig. 8($4^{th}row$)	(724,817)	2.20	5.56	2.37	2.07	2.15	**2.05**
Fig. 9($1^{st}row$)	(860,835)	20.37	6.23	4.87	60.86	6.53	**0.33**
Fig. 9($2^{nd}row$)	(426,621)	1.89	8.26	1.60	1.43	2.13	**1.31**

TABLE IV

NUMBER OF ITERATIONS OF DIFFERENT REGISTRATION METHODS FOR 2D CASES

	ICP	GMM	DT	GF	DA	PA
Fig. 8($1^{st}row$)	*20*	*30*	*14*	*26*	*13*	***10***
Fig. 8($2^{nd}row$)	*16*	*30*	*6*	*11*	*14*	***8***
Fig. 8($3^{rd}row$)	*26*	*30*	*9*	*29*	*15*	***10***
Fig. 8($4^{th}row$)	*24*	*30*	*15*	*28*	*18*	***13***
Fig. 9($1^{st}row$)	*30*	*30*	*30*	*30*	*30*	***27***
Fig. 9($2^{nd}row$)	*30*	*30*	*30*	*30*	*30*	***30***

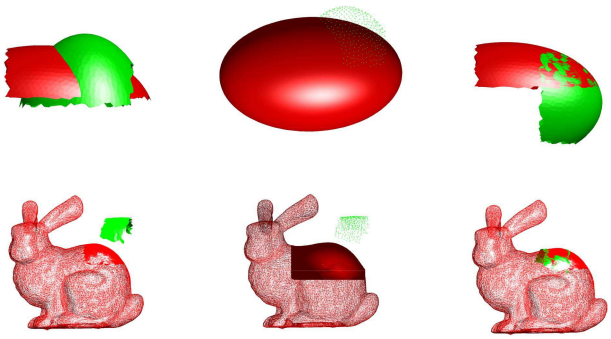

(a) *(b)* *(c)*

Fig. 9. Partial overlap cases. (*a*) Initial set up of source sets and target sets to be registered. (*b*) IPs representing target sets and the source points. (*c*) Results from the proposed approach.

in Table III, except our approach, converge to the right configuration. All these registration techniques are trapped in a local minimum, while our approach exploits the extrapolation provided by the fitted surface. The (*bottom*) row presents another illustration of partial overlap where the points are picked from the back of Bunny. In this case, although all the techniques have similar behavior, the proposed approach has the smallest ARE.

The evolution of ARE for registering Fig. 8(*bottom*) is illustrated in Fig. 10. It can be appreciated that the proposed approach has the smallest ARE and the fastest convergence. Although GF [17] reaches the same optimal ARE its convergence is slower; the oscillation in DT [15] is due to the discrete approximation of the distance field, which is not the case of the proposed approach that has a smooth behavior. The evolution of GMM is not depicted since it is out of the range of the plot.

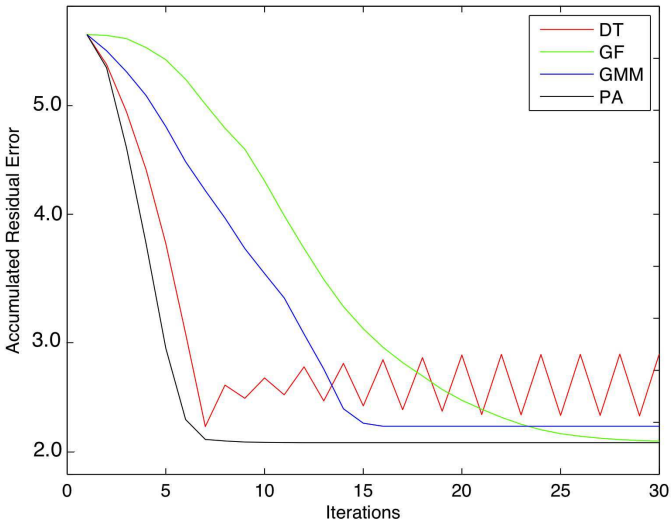

Fig. 10. Evolution of ARE of different registration algorithms along 30 iterations for registering Fig. 8(bottom).

B. Registration Using IBSs

In this section, point-to-point registration problem is converted to point-to-IBS registration where an optimal IBS represents the original target points. In order to make clearer the difference with the previous section, results are differently presented with other colors in order to highlight the fact that the target set of points is represented through an IBS that provides a more flexible representation able to tackle more challenging geometries. It is a valid alternative when IPs cannot be used (sometimes the large amount of outliers generated by IP introduce mistakes during the registration). Fig. 11 shows illustrations of the proposed approach using 2D cases. In the example presented in the first row each set contains 115 points. The contours in the other four rows are defined by 167, 174, 148 and 164 points respectively. It should be highlighted that sometimes a coarse IBS representation leads to a promising result. This can be appreciated in the examples presented in the first and third rows. In these cases, even though the IBSs do not fit the target sets accurately, the optimal registration parameters are obtained.

IBSs have been used for describing different model sets in 3D in Fig. 13. These data sets have been already used in Fig. 8 when IPs are employed for model set fitting. Fig. 12($left$) presents the initial position of source and

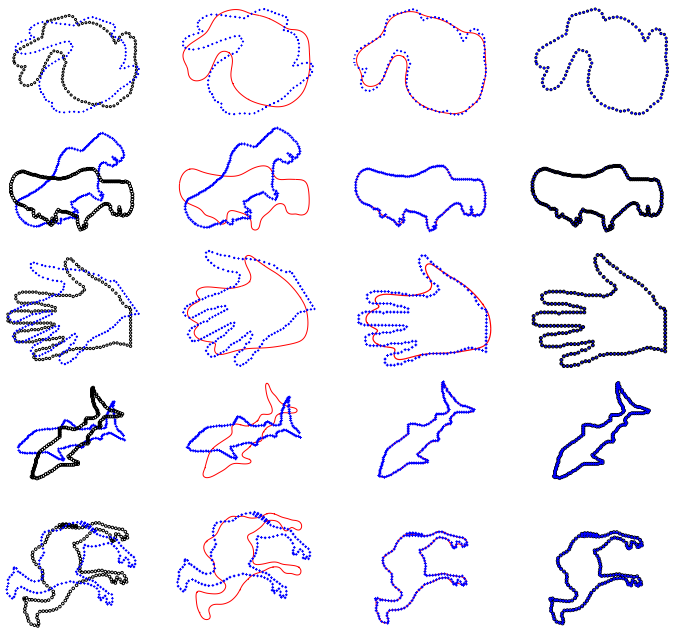

Fig. 11. (*a*) Initial positions of source (+) and target (o) sets. (*b*) Source (+) sets and IBSs representing the targets. (*c*) Final results of registered source (+) sets and IBSs. (*d*) The same result but represented by using the target (o) sets and transformed source (+) sets with the proposed approach.

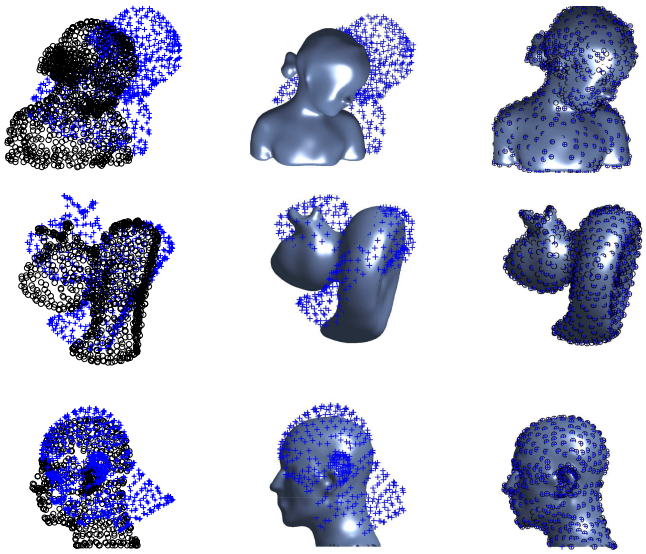

Fig. 12. Registration results using IBS for model fitting. These data has been already used in Fig. 8 for different IPs. IBSs provide more precise description compared to IPs.

target sets. Fig. 12(*middle*) shows the IBSs representing the different target sets together with the source sets. Finally, Fig. 12(*right*) presents the registration results obtained with the proposed approach; IBS surfaces used to represent target sets are just kept for visualization purpose. From the middle column in the current figure it is clear that IBSs provide more precise representation that does not suffer from the outliers. This fact benefits the registration stage when the IBS is employed for minimizing the distance between the data set and the implicit function. Table V shows the quantitative comparison between the registration results for this data set

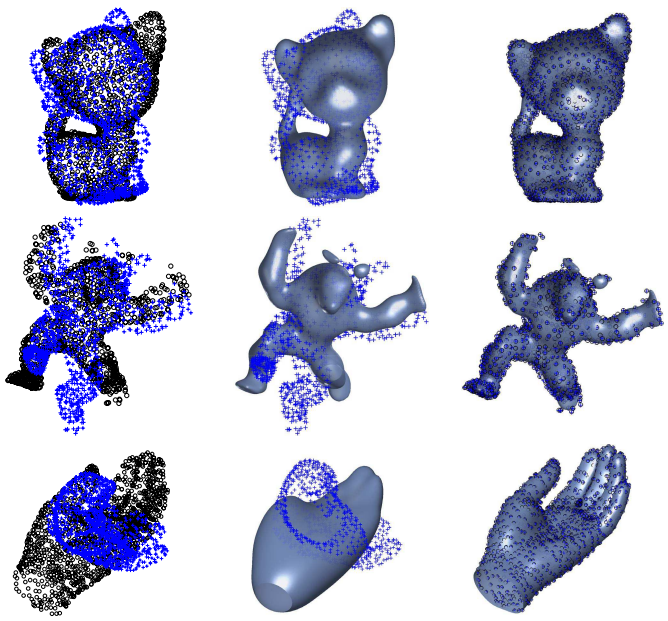

Fig. 13. 3D cases corresponding to real data sets registered with the proposed approach and state of the art techniques: (*left*) Initial positions of source (+) sets and target (o) sets. (*middle*) Source (+) and target sets represented by IBSs; (*right*) Final results of registered source (+) and target (o) sets with the proposed approach.

TABLE V
COMPARISONS OF REGISTRATION ERROR (ARE) RESULTS FOR IPS (IN FIG. 8) AND IBSS (IN FIG. 12 AND FIG. 15)

	IP	Iter.	Error		**IBS**	Iter.	Error
Bimba	7	10	3.38	—	20	7	3.05
Duck	7	8	2.74	—	20	9	2.46
Mannequin	5	10	1.90	—	25	10	1.68
Bunny	6	13	2.05	—	20	8	1.52

when different IPs and IBSs are used as interfaces. Referring to these results IBSs leads to better registration results. This fact is later studied in Fig. 15 for *Bunny* data set when different degrees of IPs and different regularizations for IBSs are employed before registration stage.

Fig. 13 presents experimental results obtained with the proposed approach when 3D data sets are considered. All the information regarding the number of points in source and target sets is provided in Table VI. These sets are obtained from the same surface but not necessarily containing the same points. Like in the 2D cases, some of the points in source and target sets are the same, which allow us to visually evaluate the accuracy of proposed approach. Note that in the cases of the "Hand" in Fig. 13(*bottom*) a *coarse to fine* approach has been used in order to reach the global minima. As shown in Fig. 13($bottom - middle$) a highly regularized IBS (consequently a coarse representation) is used at first. After five iterations, this interface has been replaced by a mildly regularized IBS (consequently more accurate representation). This IBS together with the final registration result is illustrated in Fig. 13($bottom - right$). Using IBS as an interface in our registration approach facilitates a coarse to fine registration

TABLE VI

COMPARISONS OF IBS REGISTRATION ERROR (ARE) RESULTS FOR 3D CASES (ICP: ITERATIVE CLOSEST POINT [7]; GMM: GAUSSIAN MIXTURE MODELS [13]; DT: DISTANCE TRANSFORM [15]; GF: GRADIENT FLOW [17]; DA: DISTANCE APPROXIMATION [16]; PA: PROPOSED APPROACH)

	(N_s,N_t)	ICP	GMM	DT	GF	DA	PA
Fig. 1	(240,240)	8.51	13.77	5.54	1.52	5.63	**0.06**
Fig. 13($1^{st}row$)	(1286,1557)	3.67	36.87	4.10	3.67	3.68	**3.67**
Fig. 13($2^{nd}row$)	(1007,1151)	**2.66**	49.83	2.90	5.50	2.73	2.75
Fig. 13($3^{rd}row$)	(1256,1412)	4.86	87.09	5.46	9.24	4.88	**4.85**

TABLE VII

NUMBER OF ITERATIONS OF DIFFERENT REGISTRATION METHODS FOR 3D CASES

	ICP	GMM	DT	GF	DA	PA
Fig. 1	*14*	*30*	*7*	*30*	*15*	***11***
Fig. 13($1^{st}row$)	*22*	*30*	10	*15*	*22*	***8***
Fig. 13($2^{nd}row$)	**12**	*30*	*8*	*28*	*12*	*9*
Fig. 13($3^{rd}row$)	*29*	*30*	*12*	*30*	*30*	***12***

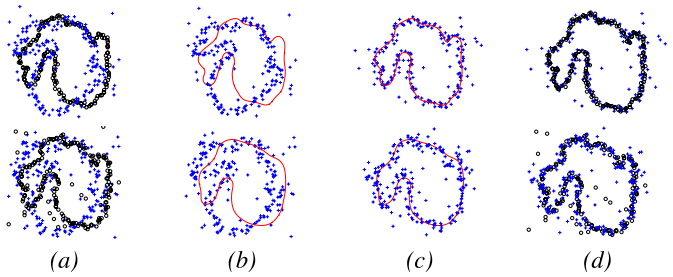

Fig. 14. The effect of outliers and noises: (a) Initial positions of source (+) and target (o) sets. (b) Source (+) sets and IBSs representing the targets. (c) Final results of registered source (+) sets and IBSs. (d) The same result but represented by using the target (o) sets and transformed source (+) sets with the proposed approach.

scheme. It should be mentioned that all we need to adjust the accuracy of IBS is the regularization parameter. For instance, in the case of Hand, the regularization parameter in eq. (14) is set to $\mu = 10^3$ when a coarse IBS is required and $\mu = 1$ when a fine IBS is replaced. Table VI and Table VII presents the registration error and the number of iterations, respectively, for all the algorithms tested during the comparisons. In all the cases the proposed approach finds the optimal parameters quite precisely, and in fewer iterations.

Our presented registration scheme easily mitigates the effect of noises and outliers. Thanks to our two-stage algorithm noise and outliers in the target and source are tackled separately in the first and second stage. Indeed, the fitting algorithm in the first stage finds the best implicit model that represents the target points. The 3L algorithm presented in section III-A is quite robust to the noise especially in the case of IBS when a high regularization parameter is used. Fig. 14 illustrates the 2D Bunny example presented in Fig. 11 disrupted by noise and outliers. In the first row the target and source points are deviated from their original position by $\pm 3\%$ and $\pm 6\%$ noise, respectively. Moreover, the source contains more than 20 outliers randomly injected in the unit square where the source lies in. The second column shows how the fitted implicit B-spline conquer the outliers effect on the target.

TABLE VIII

COMPARISON BETWEEN THE REGISTRATION RESULTS USING DIFFERENT IPS AND IBSS (THE BOLD NUMBERS ARE THOSE PARAMETERS OF IP/IBS THAT WE CHANGE FOR GOING FROM COARSE TO FINE)

	Type	Degree	λ	Iterations	Error
Fig. 15(a)	*IP*	**5**	10^{-5}	*10*	*2.27*
Fig. 15(b)	*IP*	**7**	10^{-5}	*14*	*2.01*
Fig. 15(c)	*IP*	**10**	10^{-5}	*11*	*1.92*
Fig. 15(d)	*IBS*	*20*	$\mathbf{10^4}$	*7*	*1.65*
Fig. 15(e)	*IBS*	*20*	$\mathbf{10^3}$	*8*	*1.58*
Fig. 15(f)	*IBS*	*20*	$\mathbf{10^1}$	*8*	*1.52*

Additionally, the outliers in the source are removed based on their distance comparison with the standard deviation σ_d. In the second row, the amount of noise in the target and source are increased to $\pm 5\%$ and $\pm 8\%$ respectively. In this example the target set contains around 20 outliers that are easily tackled during fitting just by employing a higher regularization. Plus, the source includes more than 40 outliers that are tackled by using a lower threshold to remove more outliers.

As already mentioned, the main goal of the first stage of our registration scheme is to come up with an interface describing the target set. This interface is in the form of an implicit function and could be either an IP or an IBS or even a RBF. As long as the function is implicit and linear with respect to its coefficient vector the 3L fitting algorithm can be applied. Fig. 15 illustrates the final results obtained by different implicit functions. The first row shows implicit polynomials of different degrees from coarse to fine and the second row includes implicit B-splines with different regularizations. Table VIII contains the information about the implicit function used for fitting, the number of iterations as well as the final registration error (with respect to a high resolution reference set). IPs and IBSs from different resolutions have been used as interface. In order to go from coarse to fine, we either change the degree (for the case of IP) or the regularization parameter (for IBS). Both qualitative and quantitative results show that a high resolution IBS leads to a more precise registration. However, starting from a low resolution implicit function and then switching to a high resolution one will help to reduce the registration error. For instance, for the case of IBS we start with a high regularization $\lambda = 10^4$ and we decrease it to $\lambda = 10^3$ and $\lambda = 10$. The decrease can happen after some iterations or when the changes in registration error (the relative error $\epsilon = |E_t - E_{t-1}|/E_t$) is too small.

In addition to the precision, IBS provides a fast distance computation in comparison with IP. In other words IPs are

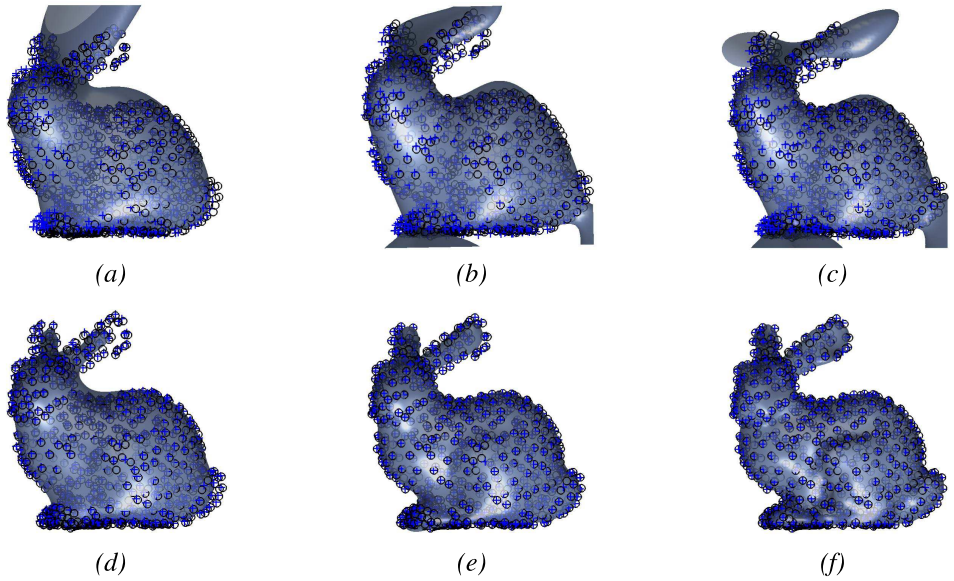

Fig. 15. Comparison between the registration results of Bunny in Fig. 8 using different IPs and IBSs. The first row correspond to IPs and the second one shows different IBSs. The description is from coarse to fine when we move from left to right.

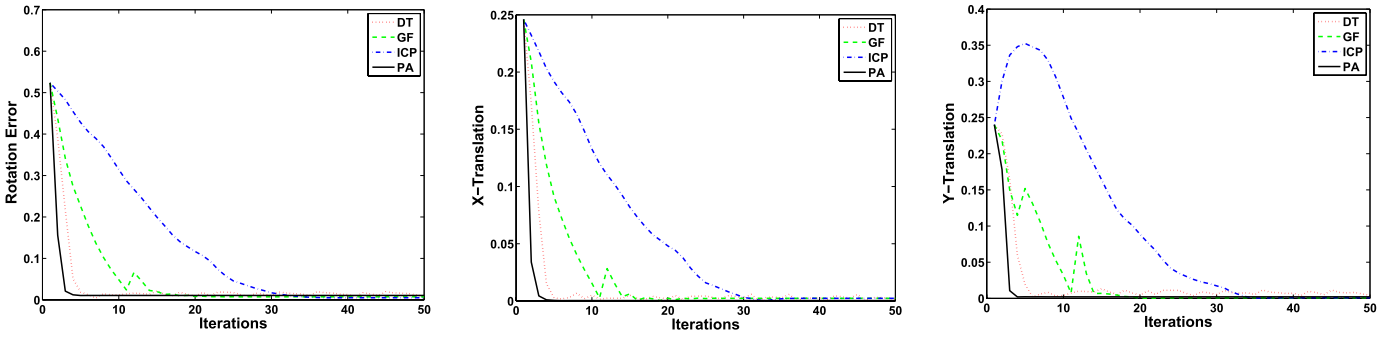

Fig. 16. Evolution of the error measurement in the parameter space for different algorithms applied for the 2D data set in Fig. 14(*top*); the errors are computed for the rotation θ and translations t_x and t_y respectively.

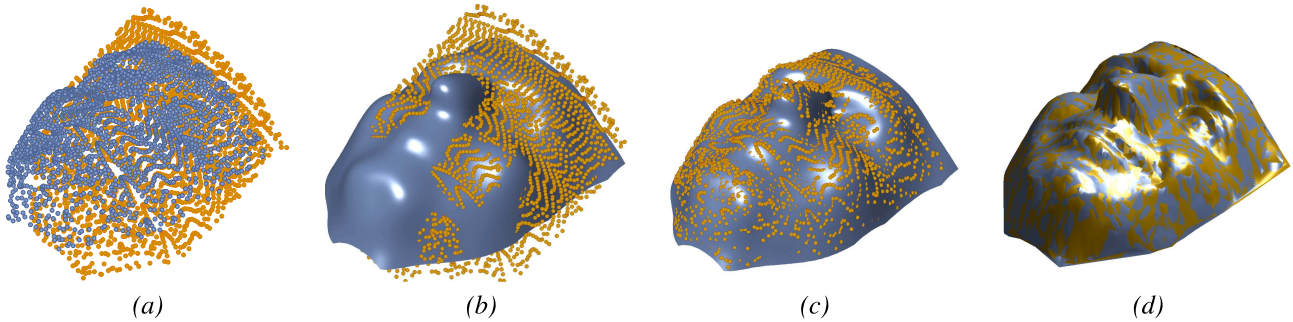

Fig. 17. Matching two different samplings of a 3D face: (*a*) Initial position of source and target sets; (*b*) Source set and target set represented by an IBS; (*c*) Registration result of source set and the IBS; (*d*) The same result but represented by triangle meshes.

much more expensive when it comes to computing the distance through our method. Computing f and ∇f for a 3D IBS takes at most 64 products to compute the inner product between the coefficients and the basis (regardless of the lattice size), while it takes 286 products when a 10th degree IP is used. Hence, IBSs are not just flexible representations but they are also cheaper for our distance estimation plus the minimization. This is the main advantage of our method when it comes to comparison with some similar work like [17]. In a non-optimized Matlab implementation, our proposed method takes around 2.1 seconds after 10 iterations to register 3D bunny data set (724 source points vs. 817 target points) with an IBS of size $20 \times 20 \times 20$ describing the target set. In contrast, a similar method like [17], which exploits IPs as interfaces, takes around 17.3 seconds after 20 iterations when just a 10th degree IP has been used to approximate the gradient field. The standard ICP method [7] takes around 13.1 seconds after 12 iterations, when a complete point to

point comparison is considered for correspondence search. The quadratic distance in [16] demands 5.5 seconds for 20 iterations with a downsampling of 10, but it requires expensive computations to estimate the principal curvatures. The method in [15] is quite fast during registration (less than 1 second for 20 iterations) but it highly depends on the distance field resolution that requires a lot of computations before starting the registration.

In all the qualitative comparisons in this manuscript we just presented the number of iterations as well as the registration errors in terms of euclidean distance between the target set and the transformed data set. However, the results could be compared in terms of the transformation parameters. Unfortunately, the distance in the parameter space does not lead to a fair comparison that is geometrically meaningful. For instance, a translated set that is two units away from the original one has the same L_1 distance as the one for a transformed set with one unit translation and rotation, while geometrically can be much further. Fig. 16 illustrates the evolution of the rigid parameters for the 2D registration problem in Fig. 14(top). The top plot in Fig. 16 illustrates the evolution of the rotation parameter while the rest two concern the translation along x and y directions. In this typical example ICP shows a slow convergence while our proposed method converges in first few iterations. As the last column depicts, ICP seems to diverges during the first five iterations, while it is converging in the geometric space. The method of discrete distance transform seems to be oscillating since it depends on the distance field resolution and it gets stuck and oscillates when it get beyond this resolution.

Fig. 17 shows two different samplings of a 3D face. Both source set and target set are sampled from a 3D scanned face. The original point cloud contains more than $112k$ points, while the sampled sets contain 2242 points. We employ an IBS with a lattice of size 20^3 and a moderate regularization $\lambda = 200$. Fig. 17(b) shows how the target set is replaced with the IBS. Then, registration is performed between the source points and the IBS model. Note that no correspondence search is applied; hence, instead of $O(N_s^2)$ comparisons only $O(N_s)$ computations for the source set with $N_s = 1242$ points are applied. In Fig. 17(c) the final alignment between the source and IBS after 12 iterations is shown. Of course, the aligned source set is not a perfect alignment of IBS, but the final figure illustrates how it perfectly matches the target set (see Fig. 17(d)).

V. Conclusion

In this paper two flexible implicit representations are exploited to tackle the registration problem. In the first stage IPs and IBSs are used to describe a cloud of points. The optimal implicit representation is obtained through a linear least squares formulation; furthermore, in the IBS case, its smoothness can be easily controlled by the regularization parameter. In the second stage we exploit the simplicity and flexibility of IPs and IBSs to propose a registration distance. Hence, the point-to-point registration problem is converted into a point-to-model one. Then, the registration problem can be tackled in different stages starting from a coarse to fine representation for the target set. Moreover, the resulting distance from the implicit function and its gradient information can be easily computed and it fits the requirement of any gradient based optimization algorithm to find the best registration parameters. Experimental results and comparisons are provided showing both fast convergence and robustness in challenging situations. Moreover, it is shown how a coarse to fine representation can lead the convergence to the global optimum.

Acknowledgment

The authors would like to thank the Associate Editor and the anonymous referees for their valuable and constructive comments.

References

[1] Y. Chen and G. Medioni, "Object modelling by registration of multiple range images," *J. Image Vis. Comput.*, vol. 10, no. 3, pp. 145–155, 1992.

[2] M. Taron, N. Paragios, and M. Jolly, "Registration with uncertainties and statistical modeling of shapes with variable metric kernels," *IEEE Trans. Pattern Anal. Mach. Intell.*, vol. 31, no. 1, pp. 99–113, Jan. 2009.

[3] M. Rouhani and A. Sappa, "Non-rigid shape registration: A single linear least squares framework," in *Proc. ECCV*, Firenze, Italy, Oct. 2012, pp. 264–277.

[4] M. Rouhani and A. Sappa, "Correspondence free registration through a point-to-model distance minimization," in *Proc. ICCV*, Barcelona, Spain, Nov. 2011, pp. 2150–2157.

[5] M. Rouhani and A. Sappa, "Implicit B-spline fitting using the 3L algorithm," in *Proc. 18th IEEE ICIP*, Sep. 2011, pp. 893–896.

[6] N. Gelfand, N. Mitra, L. Guibas, and H. Pottmann, "Robust global registration," in *Proc. Symp. Geometry Process.*, Vienna, Austria, Jul. 2005, pp. 197–206.

[7] P. Besl and N. McKay, "A method for registration of 3D shapes," *IEEE Trans. Pattern Anal. Mach. Intell.*, vol. 14, no. 2, pp. 239–256, Feb. 1992.

[8] G. Sharp, S. Lee, and D. Wehe, "ICP registration using invariant features," *IEEE Trans. Pattern Anal. Mach. Intell.*, vol. 24, no. 1, pp. 90–102, Jan. 2002.

[9] T. Zinßer, J. Schmidt, and H. Niemann, "A refined ICP algorithm for robust 3D correspondence estimation," in *Proc. ICIP*, 2003, pp. 695–698.

[10] J. Ho, A. Peter, A. Rangarajan, and M. Yang, "An algebraic approach to affine registration of point sets," in *Proc. ICCV*, 2009, pp. 1335–1340.

[11] J.-P. Tarel, H. Civi, and D. B. Cooper, "Pose estimation of free-form 3D objects without point matching using algebraic surface models," in *Proc. IEEE Workshop Model Based 3D Image Anal.*, Mumbai, India, Jan. 1998, pp. 13–21.

[12] H. Wang, Q. Zhang, B. Luo, and S. Wei, "Robust mixture modelling using multivariate t-distribution with missing information," *Pattern Recognit. Lett.*, vol. 25, no. 6, pp. 701–710, 2004.

[13] B. Jian and B. Vemuri, "A robust algorithm for point set registration using mixture of Gaussians," in *Proc. 10th IEEE ICCV*, Oct. 2005, pp. 1246–1251.

[14] F. Boughorbel, M. Mercimek, A. Koschan, and M. Abidi, "A new method for the registration of three-dimensional point-sets: The Gaussian fields framework," *Image Vis. Comput.*, vol. 28, no. 1, pp. 124–137, 2010.

[15] A. Fitzgibbon, "Robust registration of 2D and 3D point sets," *Image Vis. Comput.*, vol. 21, nos. 13–14, pp. 1145–1153, 2003.

[16] H. Pottmann, S. Leopoldseder, and M. Hofer, "Registration without ICP," *Comput. Vis. Image Understand.*, vol. 95, no. 1, pp. 54–71, 2004.

[17] B. Zheng, R. Ishikawa, T. Oishi, J. Takamatsu, and K. Ikeuchi, "A fast registration method using IP and its application to ultrasound image registration," *IPSJ Trans. Comput. Vis. Appl.*, vol. 1, pp. 209–219, Sep. 2009.

[18] M. Blane, Z. Lei, H. Civil, and D. Cooper, "The 3L algorithm for fitting implicit polynomials curves and surface to data," *IEEE Trans. Pattern Anal. Mach. Intell.*, vol. 22, no. 3, pp. 298–313, Mar. 2000.

[19] H. Dinh, G. Turk, and G. Slabaugh, "Reconstructing surfaces by volumetric regularization using radial basis functions," *IEEE Trans. Pattern Anal. Mach. Intell.*, vol. 24, no. 10, pp. 1358–1371, Oct. 2002.

[20] M. Aigner and B. Juttler, "Gauss-Newton-type technique for robustly fitting implicit defined curves and surfaces to unorganized data points," in *Proc. IEEE Int. Conf. SMI*, Jun. 2008, pp. 121–130.

[21] H. Chui and A. Rangarajan, "A feature registration framework using mixture models," in *Proc. IEEE Workshop MMBIA*, Jun. 2000, pp. 190–197.

[22] B. Zheng, J. Takamatsu, and K. Ikeuchi, "An adaptive and stable method for fitting implicit polynomial curves and surfaces," *IEEE Trans. Pattern Anal. Mach. Intell.*, vol. 32, no. 3, pp. 561–568, Mar. 2010.

[23] J. Hermans, D. Smeets, D. Vandermeulen, and P. Suetens, "Robust point set registration using EM-ICP with information-theoretically optimal outlier handling," in *Proc. IEEE CVPR*, Jun. 2011, pp. 2465–2472.

[24] S. Rusinkiewicz and M. Levoy, "Efficient variants of the ICP algorithm," in *Proc. 3rd Int. 3DIM*, May/Jun. 2001, pp. 145–152.

[25] G. Taubin, "Estimation of planar curves, surfaces, and nonplanar space curves defined by implicit equations with applications to edge and range image segmentation," *IEEE Trans. Pattern Anal. Mach. Intell.*, vol. 13, no. 11, pp. 1115–1138, Nov. 1991.

[26] R. Fletcher, *Practical Methods of Optimization*. New York, NY, USA: Wiley, 1990.

[27] (2013). *AIM@SHAPE, Digital Shape WorkBench* [Online]. Available: http://shapes.aimatshape.net/

[28] (2013). *The Stanford 3D Scanning Repository* [Online]. Available: http://graphics.stanford.edu/data/3Dscanrep/

Mohammad Rouhani (S'09) received the bachelor's degree in applied mathematics from the National University of Iran, Tehran, Iran, in 2003 and the master's degree from the Sharif University of Technology, Tehran, Iran, in 2006. Having experienced two years of lecturing in Computer Science, he joined Advanced Driver Assistance Systems Group at the Computer Vision Center in Barcelona, Spain, where he received the Ph.D. degree in Computer Vision, in 2012. After holding a research position in Computer Vision and Learning Laboratory at Imperial College London, London, U.K., he joined Morpheo team at Inria Rhone-Alpes, Grenoble, France. His current research interests include 3D Computer Vision and Computer Graphics, including shape modeling, surface reconstruction, and 3D object registration. He is also currently involved in research on machine learning techniques, including randomized decision trees applied for object detection and 3D pose estimation.

Angel Domingo Sappa (S'94–M'00–SM'12) received the electromechanical engineering degree from the National University of La Pampa, General Pico, Argentina, in 1995 and the Ph.D. degree in industrial engineering from the Polytechnic University of Catalonia, Barcelona, Spain, in 1999. In 2003, after holding research positions in France, the U.K., and Greece, he was with the Computer Vision Center, where he is currently a Senior Researcher. He is a member of the Advanced Driver Assistance Systems research group. His current research interests include a broad spectrum within the 2D and 3D image processing, stereoimage processing and analysis, 3D modeling, dense optical flow estimation, and visual SLAM for driving assistance.